

Progress in noncontact dynamic force microscopy

R. Lüthi, E. Meyer, L. Howald, H. Haefke, D. Anselmetti, M. Dreier, M. Rüetschi, T. Bonner, R. M. Overney, J. Frommer, and H.-J. Güntherodt
Institute of Physics, University of Basel, Klingelbergstrasse 82, CH-4056 Basel, Switzerland

(Received 9 August 1993; accepted 3 December 1993)

The technique of operating the scanning force microscope in the dynamic noncontact mode (dynamic force microscopy) has been improved. Home-built instruments based on an optical beam deflection scheme in two different environments were used. The two force microscopes were operated in ambient air and in ultrahigh vacuum, respectively. In order to control the oscillating cantilever different methods were applied: slope-detection (lock-in amplifier, RMS-to-DC converter) and frequency modulation (FM) technique as well. The advantages of this nondestructive technique are demonstrated on different samples, such as soft organic matter (hexagonally packed intermediate layer, Langmuir-Blodgett film), layer-structured compounds (CdI_2), *n*-doped Si(111), and ferroelectric crystals [triglycine sulfate (TGS), guanidinium aluminum sulfate hexahydrate (GASH)]. On TGS and GASH cleavage faces, the ferroelectric domains and domain walls could be imaged. From experimental data a spatial resolution of about 1–2 nm in lateral and <0.1 nm in vertical directions could be determined.

I. INTRODUCTION

Scanning force microscopy (SFM) in the attractive force regime has a variety of applications. The abbreviation DFM for *noncontact dynamic force microscopy* is suggested.¹ The term *noncontact* includes the force regime where the tip-sample interaction is dominated by the long-range attractive forces. The term *dynamic* means that the probing tip oscillates at a certain frequency, driven by an external oscillator. The attractive force regime, which is sensed by DFM, is mainly dominated by long-range forces such as van der Waals, electrostatic, magnetostatic, capillary, and hydrodynamic forces.² DFM is used to sense force gradients near the surface without surface contact. As examples, information about surface topography,^{3,4} fringing fields above magnetic samples,^{5,6} dielectric constants and potentiometry,⁷ distribution of localized charges,^{8,9} and ferroelectric domain structures^{10,11} can be obtained by DFM. Furthermore, DFM has turned out to be a promising tool to image soft biological matter without sample distortion by the sensing tip,^{1,12} and was recently successfully adapted to a liquid environment.¹³

Commonly, two detection schemes are applied to measure the force gradients: (1) the so-called *slope detection* and (2) the *frequency modulation* technique.^{14,15} Both detection schemes are briefly described in the experimental part.

In order to demonstrate the resolution power and the capabilities of DFM, some selected examples obtained with two instruments that work in different environments [ambient air and ultrahigh vacuum (UHV)] are presented in this article. Both instruments are home built and feature an optical beam deflection detector.

II. EXPERIMENT

A. Measurements under ambient conditions

The cantilever is glued onto a piezoelectric bimorph and dynamically driven close to its resonance frequency by an amplitude of 0.5–2 nm. The slope detection method was found to be the favorable detection scheme for measuring

force gradients under ambient conditions. Due to the acting force gradient the effective spring constant of the cantilever is changed and its resonance frequency modified. In the case of an attractive force gradient the resonance frequency will be lowered. Thus, keeping the oscillator frequency constant, a force gradient causes a drop in amplitude which is detected with a lock-in amplifier or RMS-to-DC converter circuit (converts all amplitude contribution into a DC signal). A feedback loop keeps the amplitude constant by adjusting the tip-sample distance. The images obtained in this operating mode are profiles of constant force gradients and can be interpreted in most cases as sample topography. Due to the hydrodynamic interaction damping can also affect the amplitude and has to be taken into account.²

B. Measurements in UHV environment

The SFM used in UHV is part of a UHV system which is equipped with conventional surface analysis methods [a combined low energy electron diffraction (LEED)/Auger optics] and a customized molecular beam epitaxy (MBE) preparation chamber.^{16,17}

Because of the much smaller damping of the cantilever in vacuum the slope detection is not suited for this environment. Therefore, the noncontact measurements in UHV were performed with a frequency modulation (FM) technique, where the shift of the resonance frequency is directly measured. For this purpose several methods apply, e.g., digital frequency counters, phase-locked loops, and FM detection. The latter two were already successfully introduced by others.^{14,15} For our studies with the DFM in UHV, we adapted a FM detection similar to that described by Albrecht *et al.*¹⁴ A separate feedback circuit is used to maintain a constant vibration amplitude of the cantilever. The resonance shift is detected by a tunable FM detector which measures the frequency-dependent phase shift in a dual inductance-capacitance (*LC*) filter. The output of the FM detector is used as the input signal for the second feedback system which regulates the tip-sample separation.

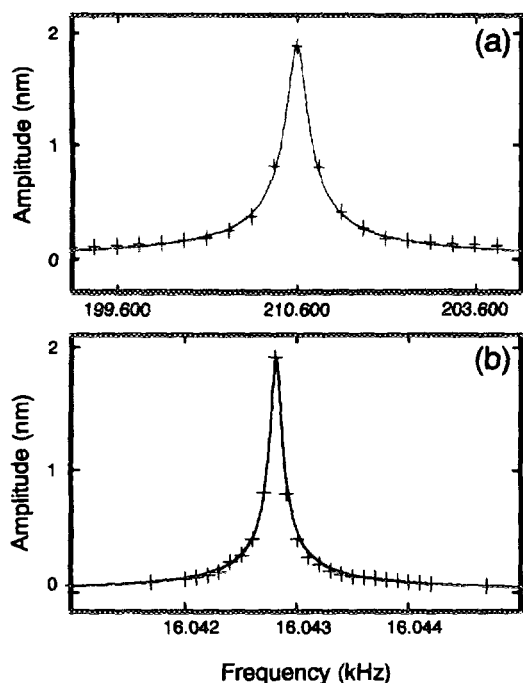


FIG. 1. Resonance curves obtained at ambient air (a) and in UHV (b). The Q factors determined from these curves are $Q_{\text{air}}=540$ and $Q_{\text{UHV}}=160\,000$, respectively.

III. RESULTS AND DISCUSSION

A. Resonance curves

Figure 1 shows two typical resonance curves, whereby the curve in Fig. 1(a) is obtained under ambient conditions and in Fig. 1(b) in UHV, respectively. Both resonance curves were fitted with the well-known Lorentzian expression

$$A(\omega) = \frac{A_0 \cdot \Omega}{\sqrt{1 + Q^2(1/\Omega - \Omega)^2}}, \quad (1)$$

with Ω as the quotient of $(\omega_0/\omega)^2$, where ω_0 is the resonance frequency, and Q is the quality factor of the resonance. The Q factors are obtained from $Q = \omega_0/\Delta\omega$ with $\Delta\omega$ measured as the full width at $1/\sqrt{2}$ th maximum of the resonance curve $A(\omega)$. Q factors extracted from curves shown in Fig. 1 are $Q_{\text{air}}=540$ and $Q_{\text{UHV}}=160\,000$ which is typical for each corresponding environment.

B. Ambient conditions

In order to estimate the resolution limits in the lateral and vertical direction of DFM two test samples were chosen: (1) an $\text{In}_{0.37}\text{Ga}_{0.63}\text{As}$ layer (IGA) and (2) a hexagonally packed intermediate (HPI) layer to test the vertical and lateral resolution power, respectively. The 900 nm thick IGA film was epitaxially grown on a (001) oriented InP wafer. HPI (hexagonally packed intermediate layer) of the bacterium *Deinococcus radiodurans* is a biological two-dimensional protein array which was prepared on a glass substrate.¹⁸ HPI was chosen because of its periodic array of protein rings with a

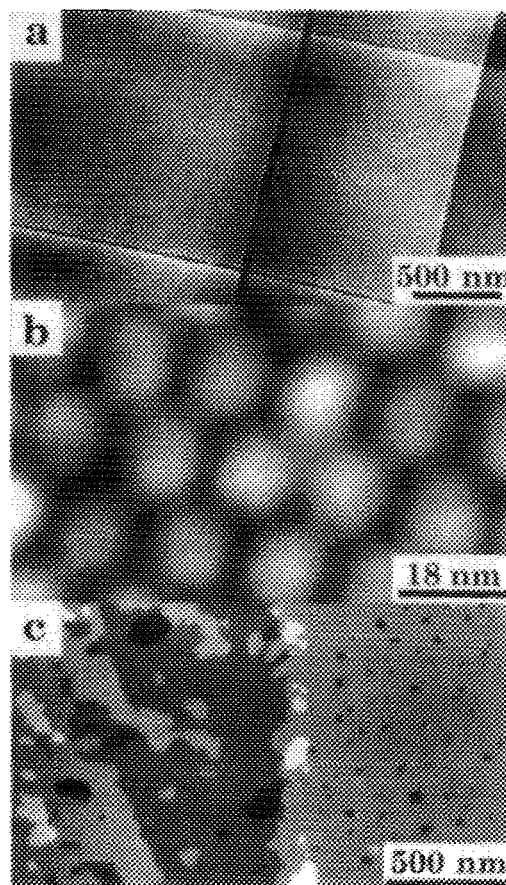


FIG. 2. Collection of force gradient maps for demonstrating the resolution power of DFM. (a) IGA. (b) HPI. and (c) LB film of Cd-arachidate.

periodicity of 18 nm, which seemed to be accessible by non-contact DFM and provided a comparison with results previously obtained by other groups.¹²

As a last sample we studied the surface of a double bilayer film of Cd-arachidate deposited by means of the Langmuir-Blodgett (LB) technique. This LB film exhibits well defined bilayer steps of about 54 Å in height. The non-contact measurements on Cd-arachidate agrees very well with contact-SFM studies, already made on the same sample system.¹⁹

Figure 2 shows a collection of DFM images obtained on the above mentioned samples. In Fig. 2(a) the IGA surface is shown revealing grooves and flat surface areas, with uniformly spaced surface steps. The height of the curved surface steps was determined to be 2–3 Å which corresponds very well with the assumed monoatomic step height of 2.5 Å. By analyzing the signal-to-noise ratio along cross sections taken perpendicular to these surface steps a vertical resolution of <1 Å was found. A detailed characterization and description of the morphology of IGA surfaces can be found elsewhere.²⁰

In Fig. 2(b) a DFM map obtained on the HPI samples is shown. The hexagonal symmetry of the HPI layer is clearly visible, where the periodicity of the protein rings agrees well

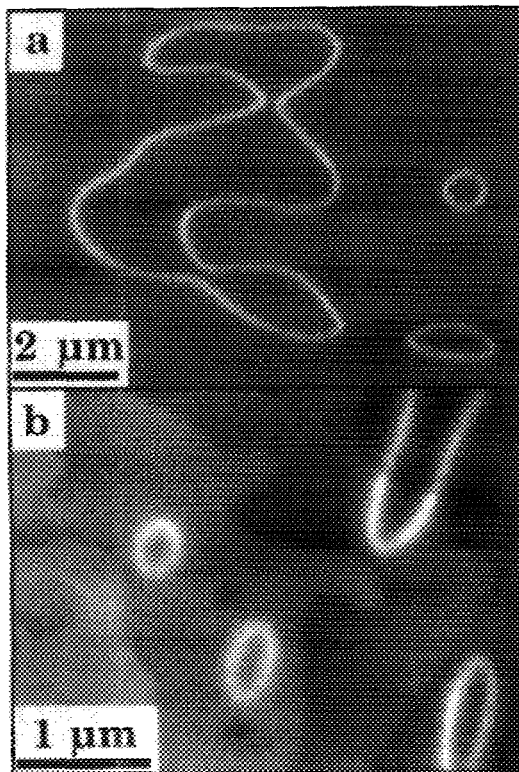


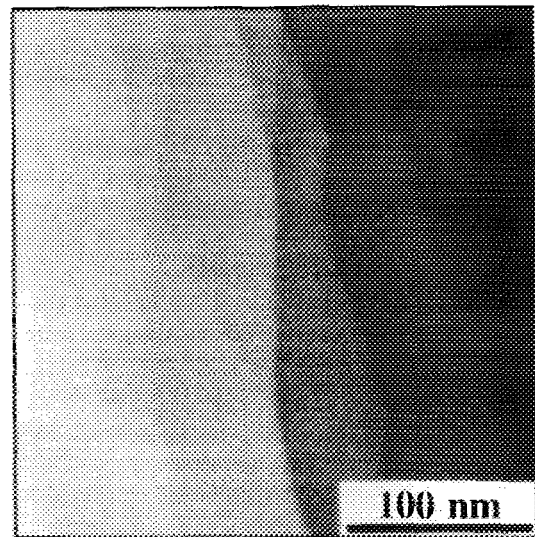
FIG. 3. Ferroelectric domain structures on ferroelectric crystals. (a) GASH and (b) TGS. The ferroelectric domain walls are revealed as bright lines.

with the value of 18 nm known from the literature.^{12,18} Furthermore, the image reveals significant details between the regions of adjoining protrusions: the interconnecting bridges (2 nm in width) of the protein rings can be identified and give an estimate of a lateral resolution limit of 1–2 nm. It has to be noted that the definition of spatial resolution (vertical and lateral resolution) is manifold in the field of microscopy. A detailed discussion related hereto can be found in a previous work.¹

The image sequence in Fig. 2(c) exhibits the surface morphology of a double bilayer of a Cd-arachidate film. Single and double bilayer steps can be identified. From the analysis of surface profiles perpendicular to the steps, the bilayer terraces were determined to be about 60 Å in height (length of the molecules forming a bilayer system is 54 Å).

HPI layers as well as LB films are known to be delicate samples under surface analysis performed with SFM, e.g., bilayers of the LB film can be easily scratched away. This often leads to imaging artifacts.¹⁹ Thus, the obtained results by noncontact DFM demonstrate impressively the nondestructive imaging capabilities, for even delicate sample materials, without losing significant resolution power.

DFM has also been found to be well suited to investigate ferroelectric domains of single crystals. Figures 3(a) and 3(b) show DFM images obtained on cleavage faces of ferroelectric crystals of GASH (guanidinium aluminum sulfate hexahydrate) and TGS (triglycine sulfate), respectively.²¹ In both images the ferroelectric domain walls are revealed as bright lines. In the case of Fig. 3(b), the domain walls are



(a)



(b)

FIG. 4. Force gradient maps obtained in UHV environment. (a) Si(111)7×7 surface, (b) the layer-structured material CdI₂.

superimposed to an eroded TGS surface. The width of the domain walls range from 50 to 80 nm, measured as the value of the full width at half-maximum (FWHM). The imaging process in DFM as well as the first results on dynamics of domains (domain dynamics as a function of annealing time and temperature) obtained by DFM are described in detail elsewhere.^{11,22,23}

C. UHV

Figure 4 documents a DFM map of a Si(111) surface measured in UHV at a base pressure of 5×10^{-11} mbar. Step heights of 3 Å were obtained which correspond to double layers of the Si(111) surface and are in agreement with data from STM images obtained by the same multiprobe microscope.⁹ The properties of the used Si(111) material as well as the applied standard procedure to prepare the Si(111)7×7 reconstruction are described elsewhere.⁹

Imaging of the Si(111)7×7 surface in the repulsive force regime by conventional contact SFM does not give images of comparable quality. Strong adhesion between tip and sample, attributed to strong interaction between unsaturated dangling bonds of the surface and probing tip, cause the tip to stick

strongly to the surface.²⁴ To overcome this problem different tip materials and/or other operation modes may be helpful to investigate the Si(111)7×7 surface and are scope of ongoing work.

As a last example a DFM map of the layer-structured material CdI₂ (the Cd atoms are sandwiched by the I atoms at a periodicity of 5.87 Å) is presented in Fig. 4(b). CdI₂ was found to be predominantly politypic and has an excellent cleavage parallel to the layers.²⁵ Figure 4(b) reveals the elementary cleavage structure on the CdI₂ surface. The crystal was freshly cleaved in UHV. The step heights were determined to be 6±1 Å in height.

In contrast to the ambient pressure measurements, the UHV measurements are not affected by hydrodynamic interaction. Thus, hydrodynamic damping can be excluded. The measured force gradients are dominated by van der Waals (vdW) and electrostatic interaction. When the contact potential is compensated, the vdW term dominates. Therefore, the presented images in Figs. 4(a) and 4(b) measured at constant vdW force gradient can be interpreted as real topographic images. Furthermore, the higher spatial resolution of DFM seems to be accessible with the application of MHz-frequency detection.²⁶

IV. CONCLUSION

The spatial resolution capability of DFM is demonstrated on selected test samples in two different environments (ambient conditions, ultrahigh vacuum). At ambient conditions (slope detection) soft organic material (HPI, Cd-arachidate) as well as hard surfaces (In_{0.37}Ga_{0.63}As layer) were successfully imaged by DFM. The resolution power was determined to be < 0.1 nm vertically and 1–2 nm laterally. In UHV (FM detection) steps on Si(111) and CdI₂ are revealed. The UHV measurements are dominated by van der Waals and electrostatic forces and are intrinsically not affected by hydrodynamic interaction. Thus, profiles measured at a constant van der Waals force gradient can be interpreted as real topographic image of the surface.

ACKNOWLEDGMENTS

We gratefully acknowledge A. Wadas and P. Grütter for many fruitful discussions, and D. Brodbeck and R. Hofer for providing us with user-friendly software. We would like to thank A. Tonin and H. Hidber for technical support and the development of the FM detector electronics. We specially thank F. Schabert and A. Engel from the Maurice Müller Institute at the Biocenter of the University of Basel for pro-

viding us with the HPI samples. This work was supported by the Swiss National Science Foundation and the Kommission zur Förderung der Wissenschaftlichen Forschung.

- ¹D. Anselmetti, R. Lüthi, E. Meyer, T. Richmond, M. Dreier, J. E. Frommer, and H.-J. Güntherodt, *Nanotechnology* (in press).
- ²M. Nonnenmacher, Ph.D. thesis, University of Kassel, GRD, 1990.
- ³Y. Martin, C. C. Williams, and H. K. Wickramasinghe, *J. Appl. Phys.* **61**, 4723 (1987).
- ⁴G. M. McClelland, R. Erlandsson, and S. Chiang, in *Review of the Progress of Qualitative Nondestructive Evaluation*, edited by D. O. Thompson and D. E. Chimenti (Plenum, New York, 1987), Vol. 6B, p. 1307.
- ⁵Y. Martin and H. K. Wickramasinghe, *Appl. Phys. Lett.* **50**, 1455 (1987).
- ⁶D. Rugar, H. J. Mamin, P. Guethner, S. E. Lambert, J. E. Stern, I. McFadyen, and T. Yogi, *J. Appl. Phys.* **68**, 1169 (1990).
- ⁷Y. Martin, D. W. Abraham, and H. K. Wickramasinghe, *Appl. Phys. Lett.* **52**, 1103 (1988).
- ⁸B. D. Terris, J. E. Stern, D. Rugar, and H. J. Mamin, *Phys. Rev. Lett.* **63**, 2669 (1989).
- ⁹E. Meyer, L. Howald, R. Lüthi, H. Haefke, *J. Vac. Sci. Technol. B* **12**, 2060 (1994).
- ¹⁰F. Saurenbach and B. D. Terris, *Appl. Phys. Lett.* **56**, 1703 (1990).
- ¹¹R. Lüthi, H. Haefke, K.-P. Meyer, E. Meyer, L. Howald, and H.-J. Güntherodt, *J. Appl. Phys.* **74**, 7461 (1993).
- ¹²W. Wiegand, M. Nonnenmacher, R. Guckenberger, and O. Wolter, *J. Microsc.* **162**, 79 (1990).
- ¹³D. Anselmetti, M. Dreier, R. Lüthi, T. Richmond, E. Meyer, J. Frommer, and H.-J. Güntherodt, *J. Vac. Sci. Technol. B* **12**, 1677 (1994).
- ¹⁴T. R. Albrecht, P. Grütter, D. Horne, and D. Rugar, *J. Appl. Phys.* **69**, 668 (1991).
- ¹⁵U. Dürig, O. Züger, and A. Stalder, *J. Appl. Phys.* **72**, 1778 (1992).
- ¹⁶L. Howald, E. Meyer, R. Lüthi, H. Haefke, R. Overney, H. Rudin, and H.-J. Güntherodt, *Appl. Phys. Lett.* **63**, 117 (1993).
- ¹⁷H. Haefke et al. (in preparation).
- ¹⁸F. Schabert, A. Hefli, K. Goldie, A. Stemmer, A. Engel, E. Meyer, R. Overney, and H.-J. Güntherodt, *Ultramicroscopy* **42–44**, 1118 (1992).
- ¹⁹E. Meyer, R. M. Overney, D. Brodbeck, L. Howald, R. Lüthi, J. Frommer, and H.-J. Güntherodt, *Phys. Rev. Lett.* **69**, 1777 (1992), and references therein.
- ²⁰H. Bluhm, F. Herrmann, R. Wiesendanger, U. D. Schwarz, and P. Paufler, *Surf. Sci.* (in press).
- ²¹The properties, preparation procedure of GASH and TGS, as well as initial results obtained with contact SFM and DFM were described in previous works, see, e.g., Ref. 11 and references therein.
- ²²R. Lüthi, H. Haefke, W. Gutmannsbauer, E. Meyer, L. Howald, and H.-J. Güntherodt, *J. Vac. Sci. Technol. B* (to be published).
- ²³H. Haefke, R. Lüthi, K. P. Meyer, and H.-J. Güntherodt, *Ferroelectrics* (in press).
- ²⁴The 7×7 reconstruction of Si(111) is commonly described by the DAS model [Dimer Adatom Stacking Fault, see, e.g., K. Takayanagi, Y. Tanishiro, S. Takahashi, and M. Takahashi, *Surf. Sci.* **164**, 367 (1985)]. In this model 19 dangling bonds per unit cell are still unsaturated and are therefore reasonably believed to be the source of strong adhesion.
- ²⁵A. A. Balchin, in *Crystallography and Crystal Chemistry of Materials with Layered Structures*, edited by F. Lévy (Reidel, Dordrecht, Holland, 1976), p. 31.
- ²⁶H. Hug, A. Moser, D. Weller, U. Dammer, I. Parashikov, A. Tonin, H. R. Hodber, and H.-J. Güntherodt, *J. Vac. Sci. Technol. B* **12**, 1591 (1993).